Stochastic Simulations of Bed Topography Constrain Geothermal Heat Flow and Subglacial Drainage near Dome Fuji, East Antarctica

Calvin Shackleton[1*], Kenichi Matsuoka[1], Geir Moholdt[1], Brice Van Liefferinge[1], and John Paden[2]

[1]*Norwegian Polar Institute, Fram Senteret, Tromsø, Norway, 9296*

[2]*Center for Remote Sensing of Ice Sheets, The University of Kansas, Lawrence, KS, USA, 66045*

Corresponding author: Calvin Shackleton ([*]calvin.shackleton@npolar.no)

Key Points:

- Stochastic simulations yield uncertainty-constrained analyses of subglacial drainage and topography-adjusted geothermal heat flow (GHF).
- Order-of-magnitude rougher bed than previous work shows widespread local GHF variability, impacting regional-mean and bed conditions.
- New empirical relationship derived to implement bed-elevation uncertainty into radar survey planning for varying bed roughness.

Abstract

Dome Fuji, inland East Antarctica is one of only few regions where 1.5-Ma old ice can be preserved for investigating the mid-Pleistocene Transition. We used stochastic simulation and various radar datasets to generate a bed topography ensemble with the continuous, realistic roughness necessary to assess basal conditions. Ensemble analysis reveals the magnitude and spatial distribution of topographic uncertainty, facilitating uncertainty-constrained assessments of subglacial drainage and topographic adjustments to geothermal heat flow. We find that topographic variability can lead to widespread local geothermal heat flow variations of ± 20% the background value, which aggregate to raise the regional value and suggest previously underestimated distributions and rates of basal melting. We also find that survey profile spacing has an increasing influence on topographic uncertainty for rougher bed, deriving an empirical relationship that could guide future survey planning based on uncertainty tolerance.

Plain Language Summary

The landscape beneath ice sheets affects ice flow, melt and refreeze at the base, subglacial drainage of meltwater, and presence of very old ice near the base which can be used for climate reconstruction. Dome Fuji, inland East Antarctica is one of few candidate sites for drilling an ice core that covers a major climatic change around 1 million years ago. Using ice thickness measurements from airborne and ground-based radar surveys with 0.25 – 10 km spacings, we simulated values between measurements to produce 100 possible continuous grids of the landscape beneath Dome Fuji. For each result we estimate the impact of valleys and ridges on geothermal heat distribution and predict water flow directions and lakes that store basal meltwater beneath the ice sheet. Averaged results show where processes are most likely to occur while also indicating uncertainty. We find that landscape variability beneath the ice sheet could increase the distribution and rates of deep ice melting. The uncertainty analysis we applied could also be used to assist the planning of future surveys aiming to map the landscape beneath thick ice in this region and elsewhere in Antarctica and Greenland.

1 Introduction

Subglacial topography drives fundamental ice sheet processes yet remains a persistent source of uncertainty across a broad spectrum of glaciological research. Resolving bed elevation at an appropriate scale is necessary to investigate the spatial distributions and sensitivities of basal ice temperature, subglacial melting, water flow and ponding. For example, current geothermal heat flow (GHF) models for Antarctica resolve variability at scales >10's of kilometres (Reading et al., 2022), resulting in model estimates that over half the Antarctic Ice Sheet bed is at the pressure melting point (Pattyn, 2010; Van Liefferinge and Pattyn, 2013). However, spatial variability in GHF at <10 km-scales modulated by bed roughness can induce local GHF variations up to twice the regional value (Colgan et al., 2021; van der Veen et al., 2007). Modelling investigations show that locally-varying GHF fields produce more meltwater than a constant GHF representing the regional mean (McCormack et al., 2022). Beneath inland ice there is insignificant frictional heating from basal sliding, amplifying the importance of GHF for basal ice temperatures.

Dome Fuji, inland East Antarctica is a candidate site for the preservation of ice over 1.5 Ma that could provide continuous climate records spanning the mid-Pleistocene Transition (Fischer et al., 2013). Constraints on GHF and subglacial hydrology are crucial in this region for characterising 1.5 Ma ice and understanding catchment-scale ice dynamics. At the interior of ice sheets where ice surfaces are relatively flat, bed topography mostly controls meltwater drainage (Shreve, 1972). Basal meltwater flows in extensive drainage networks (Dow et al., 2022), is stored in and released from subglacial lakes (Livingstone et al., 2022), and accretes onto the base of the ice sheet (Bell et al., 2011). Here, we compiled multiple ice-penetrating radar datasets to constrain ice thicknesses and investigate the bed beneath Dome Fuji (Figure 1a). The region has complex topography with mountains and valleys (Karlsson et al., 2018; Tsutaki et al., 2022), evidence for subglacial lakes (Karlsson et al., 2018; Popov and Masolov, 2007; Siegert, 2000), and estimated near-basal temperatures at the pressure melting point (Talalay et al., 2020). This indicates a potential for sensitive basal conditions and active hydrological systems, emphasizing the need for constraining the impacts of topographic variability and uncertainty.

2 Methods

2.1 Ice thickness data

Ice-thickness data were compiled from (Figure 1a): ground-survey data collected by a Japan-US-Norway collaboration and processed by the Centre for Remote Sensing of Ice Sheets (CReSIS), University of Kansas (Rodriguez-Morales et al., 2020); ground-survey data collected since 1992 by Japan's National Institute of Polar Research (NIPR) during Japanese Antarctic Research Expedition (JARE) 33-60 (Tsutaki et al., 2021a-i); airborne geophysical surveys conducted by the Alfred Wagener Institute's (AWI) Oldest Ice Reconnaissance (OIR) campaign (Eisen et al., 2020) and Geodynamic Evolution of East Antarctica (GEA) project (Eagles et al., 2021). At locations where data are not available within 10 km, background values were supplied by extracting Bedmap2 (Fretwell et al., 2013) data points and sampling BedMachine2.0 (Morlighem et al., 2020). See Supporting Information S1.1 for full details.

Two-way travel time to depth conversions for ice-bed picks were standardised (*Supporting Information S1.2*) between datasets using a radio-wave propagation speed of 1.69 x 10^8 m s^{-1}, a depth-averaged assumption applied previously in this region (Tsutaki et al., 2022). The ice-thickness datasets were compared at 783 crossover points, yielding median differences -1 m, 3 m, 18 m between CReSIS data and AWI, JARE59, JARE60 respectively (*Supporting Information S1.3*).

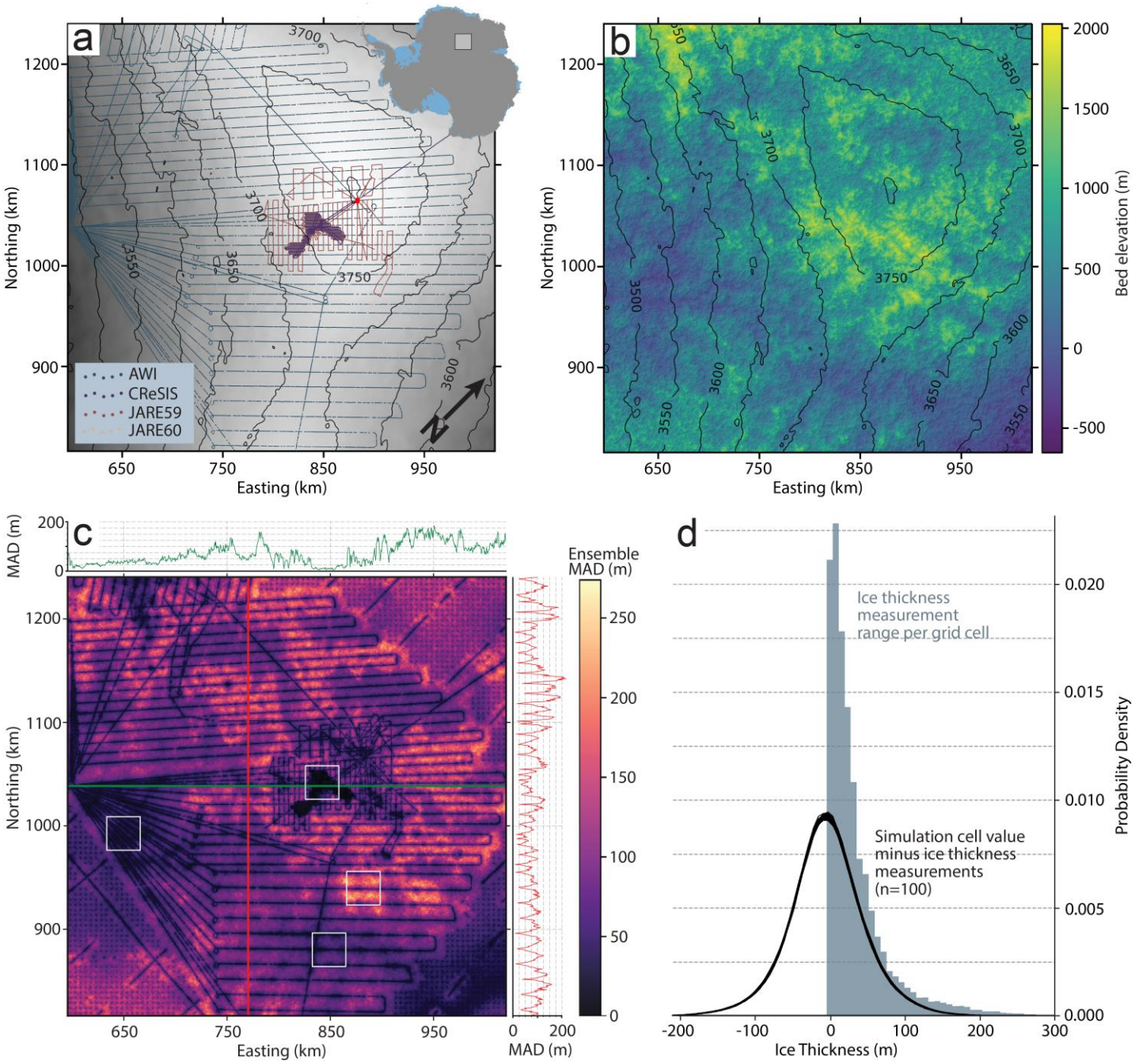

Figure 1. Bed topography simulations and analysis. **a)** Radar survey tracks, Dome Fuji Station (red diamond) and REMA ice surface contours (Howat et al., 2019). **b)** Hillshaded bed simulation #001 from the ensemble. **c)** Median absolute deviation (MAD) between 100 results with vertical and horizontal profiles plotted. Four boxes indicate sample locations (Section 4.3). **d)** Simulated bed minus measured ice thickness (100 curves) and measurement range within each map grid cell (bars). All maps projected to EPSG: 3031 with elevations in meters referenced to the WGS84 ellipsoid.

2.2 Stochastic simulation of bed topography

Sequential Gaussian Simulation (SGS) is a stochastic method (Deutsch and Journel, 1997) that can be applied to simulate values between measurements based on the statistical characteristics of nearby data (e.g. Graham et al., 2017; Law et al., 2023; MacKie et al., 2021, 2020). The SGS algorithm moves sequentially over a random path on a 2D grid, selecting values for unsurveyed grid cells using a Gaussian probability function. The probability distribution is generated using a local mean and semi-variogram estimated from a statistical model, and conditioned by surrounding data points which are sequentially updated with previously simulated values. We empirically determined optimum parameters for the exponential model based on the experimental semi-variogram (*Supporting Information S2)*.

Ice-thickness data were decimated to 100 m spacing using a median reduction filter, and the SGS algorithm was implemented using 40 nearby conditioning data points within a search radius of 30 km to simulate values for cells without measurements. We used SGS to generate an ensemble of 100 ice-thickness grids, and bed elevation was estimated by subtracting ice thicknesses from the Reference Elevation Model of Antarctica (REMA) ice-surface elevation (Howat et al., 2019).

2.3 Topographic modification of geothermal heat flow

To simulate the impacts of topographic relief on GHF distribution, an adjustment factor for large-scale GHF fields was calculated following an empirical geostatistical approach (Colgan et al., 2021). A function for the unitless local topographic modification to GHF (ΔG/G) was calculated:

$$\left(\frac{\Delta G}{G}\right)_{i,j} = \frac{1}{\alpha}\left(\bar{z}_{i,j} - z_{i,j}\right), \quad (1)$$

where G = modelled large-scale GHF estimate, α = empirically-determined local topographic relief required to induce 100% change in local GHF, z = local bed elevation, $\bar{z}$ = mean elevation averaged over an empirically determined horizontal radius *r*, and i, j = two-dimensional horizontal grid indices. We used parameterisations α = 950 m and *r* = 5 km based on a synthesis of parameter combinations against both observed and modelled local GHF anomalies that arise from topographic relief (Colgan et al., 2021).

2.4 Subglacial water flow and ponding

Subglacial hydraulic pressure potential (ϕ) was estimated for each simulated bed following Shreve (1972). We assumed that water pressure equals ice overburden pressure, a steady-state assumption appropriate for inland Antarctica where high-pressure distributed water systems are generally maintained between channels (Dow et al., 2022). Water routing was determined for gradients in ϕ using a D∞ algorithm (Tarboton, 1997). Locations of hydraulic sinks were used to predict potential sites of subglacial lakes, and spill points provided a proxy for lake depths. Hydraulic sinks generated through stochastic simulation can be artificial at grid cells far from measurements, so median lake depth over the ensemble was used to screen for persistently predicted sites of water ponding.

3 Results

3.1 Bed elevation, variability and uncertainty

We generated an ensemble of n = 100 ice thickness and bed elevation grids (Shackleton et al., 2023) which have elevations between -500 m and 2100 m. An example result (#001) is presented in Figure 1b and all results are presented in Movie S1. Steep, mountainous terrain with valleys and ridges occurs at a subglacial massif south of Dome Fuji Station, with smoother terrain directly beneath and north of the ice dome and in lowland valleys converging to the southwest. Regional subglacial topography described in previous work (Fujita et al., 2012; Karlsson et al., 2018; Tsutaki et al., 2022) are observed in the results.

The median absolute deviation (MAD) for the bed topography ensemble stack quantifies the variability between simulated topography (Figure 1c) and has a regional average of 85 ± 41 m (mean [μ] ± 1 standard deviation [σ]). Areas with radar data are distinct with low MAD, with close to zero variability near dense survey profiles over the subglacial massif, and less than 25 m in the vicinity of other survey profiles. Less than 50 m variability is typically observed within 2 km of measurements, increasing to over 250 m between the most widely spaced survey profiles (10 km spacing). Measured topographic variability also influences MAD, which is high close to rough bed and generally below 100 m in smoother regions.

Individual results were validated by calculating the difference between ice-thickness measurements (before median filter decimation) and simulated ice-thickness grid cell values extracted at measurement locations (*Supporting Information S3.1*). Probability density functions for all validation results show little variability (Figure 1d), indicating that error distributions remain consistent across the ensemble. The ensemble mean difference is close to zero but distributed widely (0.9 ± 50.7 m). However, the range of observed ice-thickness within each grid cell is comparable at 37.2 ± 44 m (Figure 1d), suggesting that the uncertainty of simulated topography is similar to measured variability within individual grid cells.

3.2 Topography-adjusted geothermal heat flow

Bed topography grids were used to estimate local topographic adjustments to GHF (Shackleton et al., 2023), calculating a unitless adjustment factor ΔG/G for large-scale GHF fields (Figure 2a; Movie S2). The adjustment factor can be ± 40% in regions with high topographic relief, with little to no adjustment in regions of smooth bed. At 10's of km-scale, adjustments show GHF is reduced along ridges and increased along valley floors (Figure 2b). The probability density functions for adjustment factors over ensemble results show negligible variation (Figure 2c) reflecting consistent regional roughness patterns. The regional impact of topographic adjustments therefore remains consistent between results, and ensemble median of 0.6% suggests elevated GHF is expected, with local adjustments mostly ± 20% (2σ).

Regional GHF estimates differ substantially between published pan-Antarctic models, as shown in Figure S8 (An et al., 2015; Burton-Johnson et al., 2020; Lösing and Ebbing, 2021; Martos et al., 2017; Purucker, 2012; Shen et al., 2020; Stål et al., 2021). At Dome Fuji Station values range 40.0 - 63.7 mW m^{-2} (Figure 2d). Our topographic GHF adjustments at the core site are between -6.5% and 10.2% over the ensemble (Figure 2e) but are predominantly positive at 2.8 ± 3.1% (1σ). By applying this adjustment factor to a local GHF of 78.9 ± 5.0 mW m^{-2} estimated from borehole temperatures (Talalay et al., 2020), we inversely estimate an adjusted regional value of 76.7 mW m^{-2} in the vicinity of Dome Fuji Station.

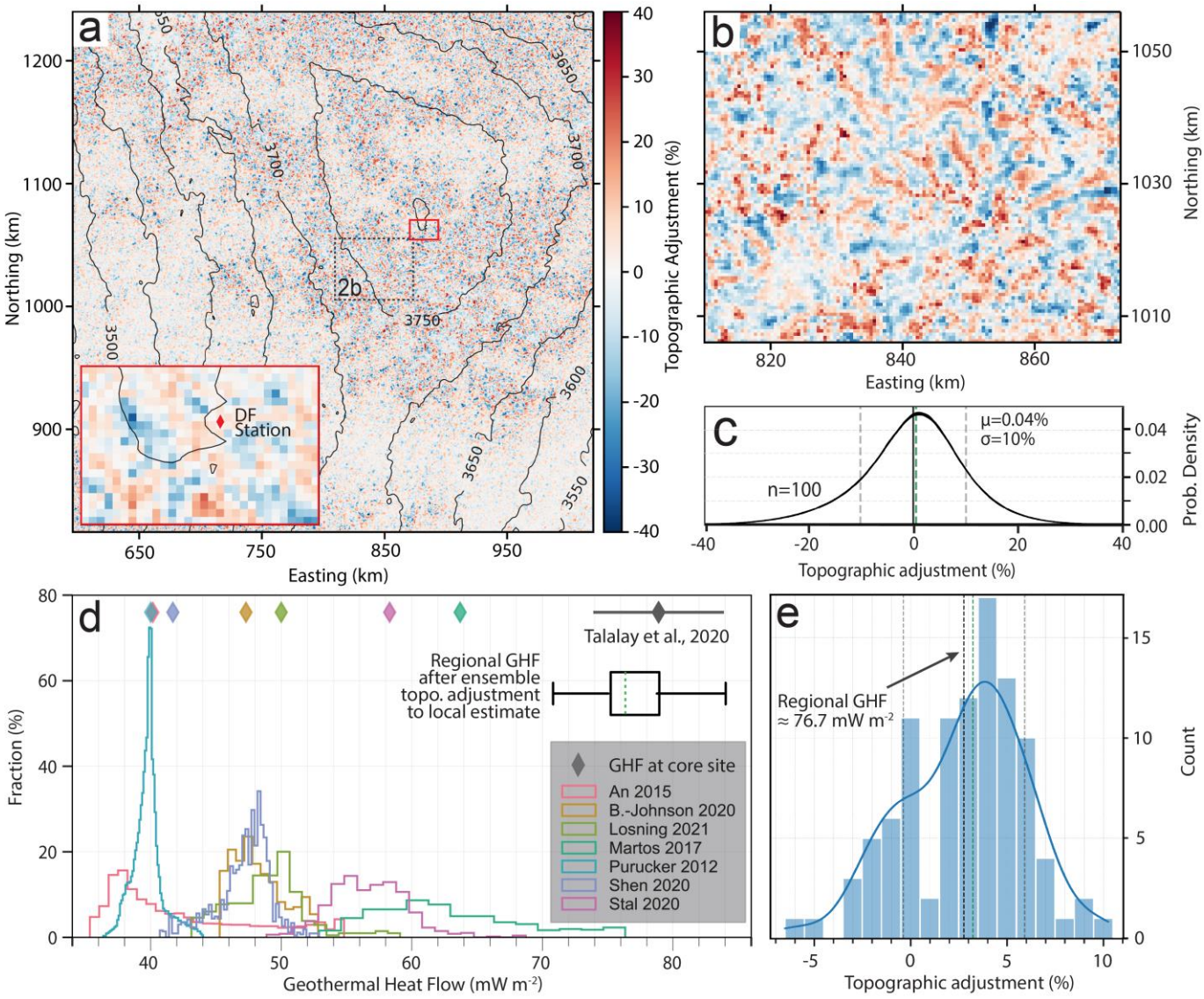

Figure 2. Spatial variations in GHF. a) Topographic adjustments to GHF (result #001) and inset a 10 x 15 km region (red box) around Dome Fuji Station. b) The central subglacial massif (result #001). c) Probability density curves for 100 topographic adjustment results, with ensemble-averaged standard deviation (grey), mean (black) and median (green). d) GHF distributions in the study region from pan-Antarctic models and corresponding value at Dome Fuji Station (diamonds). Local GHF estimate (Talalay et al., 2020) in grey, with box plot showing potential regional GHF range after ensemble adjustments to local value. (e) Topographic adjustment factor over the ensemble at Dome Fuji Station, with ensemble-averaged mean (black), median (green) and standard deviation (grey).

3.3 Meltwater drainage and subglacial lakes

Our analysis predicts dendritic networks of streams routing water away from central sectors and the subglacial massif, broadly conforming to ice drainage divides at the regional scale and mostly following bed topography at <10 km scale (Figure 3). Dense grouping of predicted streams indicates consistent water-flow predictions, more commonly associated to regions with dense measurements for example at lower elevations in ice-drainage basin-3 (B3 in Figure 3). Spatially distributed stream predictions are ubiquitous and occur between otherwise stable stream networks, for example at Easting 700 km, Northing 1050 km where inconsistent water routing coincides with a larger gap between survey profiles (Figure 1a). Other regions contain inconsistent water routing despite regular spacing between profiles, coinciding with high topographic uncertainty where streams diverge around an obstacle (e.g., northern B10) and low topographic uncertainty within lowlands (e.g., southern divide of B3/B10). Ensemble analysis indicates potential sites for subglacial lakes at the bed which have ensemble median depths up to 27 m and extents ranging from 0.25 – 395 km^2. Using ensemble median values excludes infrequently predicted lakes in interpolated regions, resulting in more lakes near survey profiles.

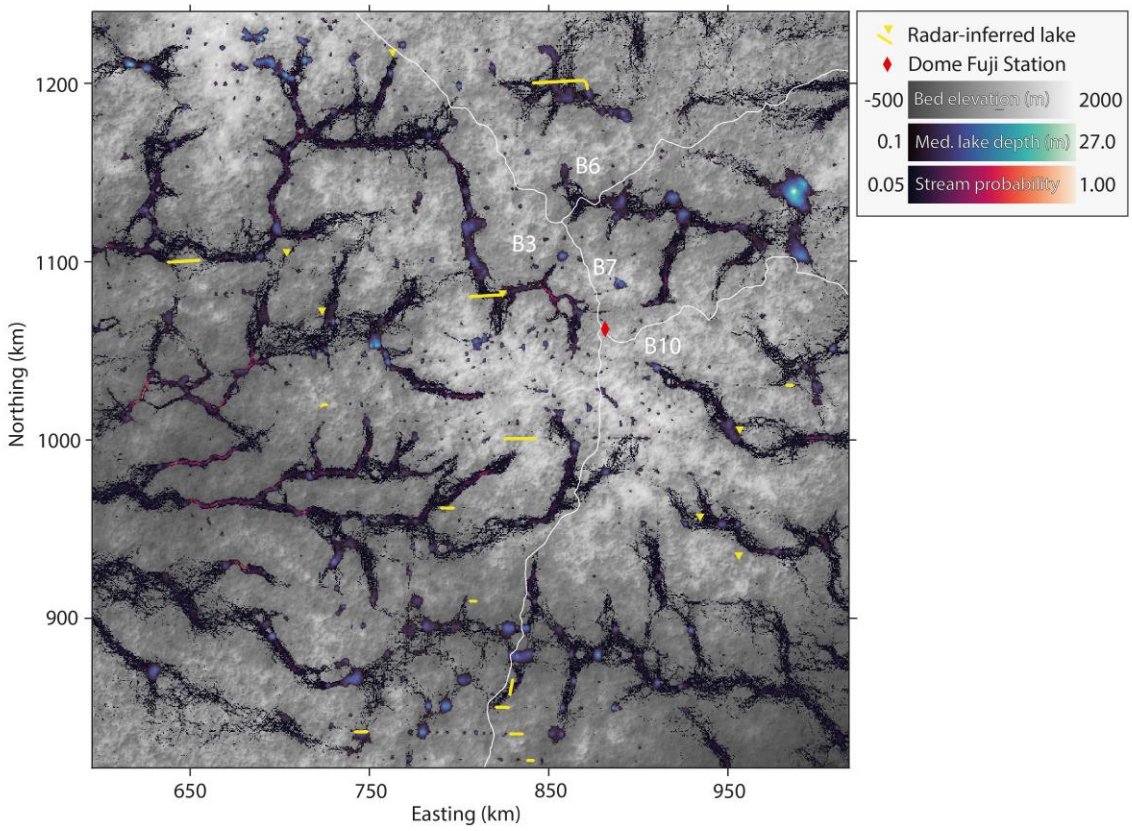

Figure 3. Subglacial drainage predicted over the bed topography ensemble. Stream probability (> 0.05) and ensemble median lake depths (> 0.1 m) over a hillshaded bed elevation map (result #001). Radar-inferred subglacial lakes as yellow triangles at lake center coordinates (Siegert et al., 2005) or lines along-profile (Karlsson et al., 2018). Ice sheet drainage basins delineated and labelled in white from Zwally et al., (2012).

4 Discussion

4.1 Topographic variability and subglacial processes

All topographic features with scales of 10's km are consistently observed across the ensemble, and regional patterns of GHF adjustments and subglacial water drainage remain consistent. The exact geometry and location of <10 km-scale topography can vary between simulations (Movie S1) and local-scale features are affected by topographic uncertainty (Figures 2a, 3), which is highest where the bed is rougher and/or measurement density is lower (Figure 1c). To examine variability in short-scale bed roughness we calculated the Terrain Ruggedness Index (TRI), which takes the square root of sum of squared differences between grid cells and 8 surrounding cells (Riley et al., 1999). Region-wide TRI has consistent distributions between simulated beds (Figure 4a), with ensemble median 213 ± 117 m (1σ). The regional mean TRI for the same domain in Bedmachine v3 is 34 ± 28 m (1σ) and Bedmap2 is 46 ± 36 m (1σ), suggesting that bed topography in this region could be an order-of-magnitude rougher with larger GHF variability than shown in other interpolated bed topography maps.

Subglacial drainage analyses predict potential locations and extents of subglacial lakes and show drainage sensitivities to topographic uncertainty (Figure 3). There are 20 subglacial lakes inferred from radar data in this region (Karlsson et al., 2018; Livingstone et al., 2022; Wright and Siegert, 2012), of which 11 directly coincide with our ensemble median lake predictions. Radar-derived bed elevation inherently masks the bathymetry of radar-detected lakes, so the topography analysis in this study is unlikely to predict all radar-detected lakes in bankfull condition. Of the 9 radar-inferred lakes that are not predicted in this study, 4 are located upstream of consistently predicted streams which delineate drainage pathways. Uncertainty-constrained subglacial water flow directions also outline any potential connectivity between drainage systems and across catchments that otherwise might not be detected using a single bed interpolation. We identified several drainage pathways across the continental ice-flow divides which reflect regionally low ice-surface slopes, and predicted lakes close to grid-south have uncertain drainage towards either Basin-3 or Basin-10. The topographic uncertainty analyses reveal regions where an ensemble approach to predicting subglacial processes could be necessary or more data is needed to reduce uncertainty, especially important in regions where basal conditions are sensitive to topographic variability.

4.2 Basal conditions and presence of 1.5 Ma old ice

Diagnosing basal conditions is crucial for deep ice core site selection, and our topographic adjustments to GHF show sensitivity to km-scale physiographic settings. Thermodynamical modelling suggests 3.1% of our study area had frozen bed for the past 1.5 Ma which could preserve old ice (Van Liefferinge et al., 2018). Regionally elevated GHF and local variability indicate that using large-scale GHF models may lead to inaccurate estimates of thawed bed and basal melt rates. The subglacial massif is well-constrained by measurements, and we consistently estimate local GHF adjustments up to ± 30%. The DF2 core was drilled in a locally elevated GHF region ca. 3% higher than background values, equating to 2.2 mW m^{-2} using the Talalay et al., (2020) estimate. Many localities even within 10 km of the previous site could have topographically adjusted GHF over 5% lower (Figure 2a), a crucial difference here where basal temperatures are close to or at the pressure melting point.

Over the subglacial massif, Van Liefferinge et al., (2018) estimated the threshold GHF required to keep basal ice frozen over the past 1.5 Ma is ca. 65 mW m^{-2}, which can be lowered to 55 mW m^{-2} considering new surface mass balance data averaged over the past 300 years (Van Liefferinge et al., 2021). Some pan-Antarctic models show that the revised threshold is met over the subglacial massif, but do not replicate local GHF derived from borehole-temperatures despite our topographic adjustment factor (Figure 2d). Previous borehole-based GHF estimates using an ice thickness of 3090 m reported earlier (Dome-F Deep Coring Group, 1998) were lower at 59 mW m^{-2} (Hondoh et al., 2002) and 50.4 mW m^{-2} (Mony et al., 2020). A revised ice thickness of 3028 ± 15 (Fujita et al., 2006) was used by Talalay et al., (2020) for their estimate of 78.9 ± 5.0 mW m^{-2}. Our data compilation suggests radar-derived ice thicknesses within 500 m of the DF1 core site are 3018 ± 16 m (1σ), based on averaged values from 4 independent surveys (Table S2), supporting the larger GHF estimates around Dome Fuji Station.

Simulated bed topography with robust uncertainty constraints indicate that local relief is not a significant control on the current ice dome location, implying that the location could have been different in the past. Thermomechanical modelling suggests that ice thicknesses could have fluctuated up to 250 m near Dome Fuji over the last 800 ka (Parrenin et al., 2007). Re-routing of water between catchments is plausible with shifting overlying ice, and historical water storage and drainage patterns could vary significantly from present-day conditions, which could affect delineation and characterisation of 1.5 Ma old ice. Meltwater refreezing onto basal ice also has significant potential to disturb basal ice stratigraphy, as observed in the nearby Gamburtsev Mountains (Bell et al., 2011). Our bed topography ensemble could be utilised further to constrain potential basal ice flow disturbances to layer stratigraphy through ice flow modelling.

4.3 Survey spacing required for a given bed uncertainty tolerance

The wide-ranging radar survey spacings in this region (0.25 - 10 km) allowed us to explore the relationship between distance d from radar data, bed roughness (TRI), and topographic uncertainty (MAD). Based on ensemble-averaged TRI and survey locations we manually identified regions that have characteristically rough and smooth bed with both dense and sparse measurements (Figure 1c: white boxes). TRI in these regions is distinct across the ensemble (Figure 4a). MAD increases for increasing d but plateaus for $d > 6$ km, at ca. 200 m for rough bed and ca. 75 m for smooth bed (Figure 4b). Both examples with distinct data density show similar distance dependencies for MAD, which implies a bed-roughness-dependent relationship between topographic uncertainty and survey spacing. Regression analysis between TRI and MAD for data grouped into 0.5 km d intervals for 0 km < d < 10 km (Figure 4c) demonstrates that MAD increases with TRI for each d interval, and the rate of increase is enhanced for larger d. Linear models were fit to binned data with y-intercept fixed at zero assuming MAD approaches zero for smooth surfaces, showing that MAD ≈ βTRI, where β represents the dependence of topographic uncertainty on bed roughness.

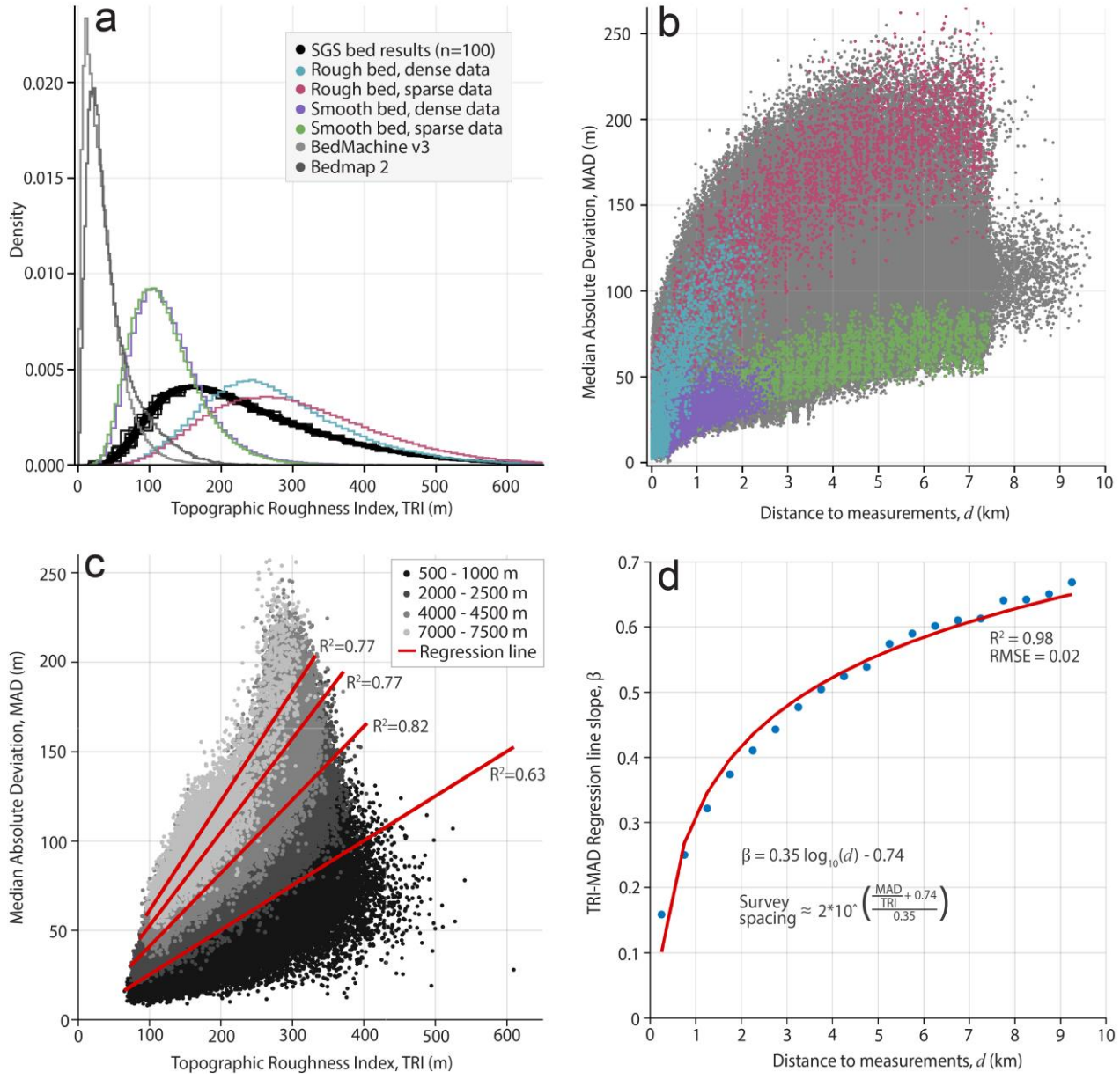

Figure 4: Topographic uncertainty dependence on bed roughness and survey spacing. **a)** Topographic Roughness Index (TRI) in the Dome Fuji region, for ensemble results (black curves), sample regions shown in Figure 1c, Bedmachine v3, and Bedmap2 at native resolution. **b)** Median Absolute Deviation (MAD) at increasing distances from measurements. Characteristic regions plotted in same colours as 4a, with all other locations in gray. **c)** MAD for increasing TRI binned at 0.5 km *d* intervals between 0 and 10 km. Only 4 of the 19 intervals are plotted to show overall trends, with full model statistics in Table S3. **d)** Slopes of fitted regression lines in 4c, at increasing distance to measurements.

Figure 4d shows the distance dependence for β, and the empirical relationship could be used to guide survey planning given an initial estimate for regional roughness based on existing data or preliminary surveys. Interpolated grids based on sparse data lack roughness between survey profiles and are not suitable for preliminary roughness analyses. Using a derived TRI, the separation between survey profiles (i.e. twice the distance to data points, *2d*) can be prescribed for a given uncertainty tolerance (Figure 4d). If bed roughness is similar to the Dome Fuji region (median TRI = 213 m), survey profiles should be separated by 1.2 km, 5.7 km, 27 km for an uncertainty tolerance of 50 m, 100 m, 150 m respectively. Considering TRI σ of 117 m the previous survey spacings are reduced to 0.7 km, 1.9 km, 14 km however for TRI of 330 m. Although it is difficult to accurately estimate bed roughness prior to extensive surveys, this relationship could be used to empirically implement scientific requirements into survey planning. Bed topography mapping guided by uncertainty tolerance might be particularly useful in coastal regions of Antarctica, where uncertainty could impact estimated ice discharge and projected grounding-line retreat of fast-flowing glaciers. To develop this approach further the measurement scale and bed roughness metric should be investigated as well as the impacts of grid cell size. New pan-Antarctic datasets (Frémand et al., 2022) could facilitate analyses of this relationship for different regions and glaciological settings.

5 Conclusions

Stochastic simulations provided detailed bed topography with realistic roughness an order-of-magnitude larger than previous interpolations. Topographic uncertainty is significantly larger in regions with rougher bed, and we quantified the dependence of topographic uncertainty on distance to radar measurements and bed roughness. An empirical relationship can guide the spacings of future surveys in the Dome Fuji region and could be applied and developed elsewhere to plan surveys within a framework of uncertainty tolerance. Constraining the bed to within 50 m requires radar profile spacings of 0.7 km to 1.2 km in this region. The impacts of topographic variability on the distribution of GHF and subglacial drainage were investigated through ensemble analysis of simulated beds. Topographically adjusted GHF is elevated in valleys and reduced over ridges, with km-scale variability leading to widespread local GHF adjustments ± 20% the regional value, aggregating to enhance overall GHF. These effects could strongly regulate the distribution of basal ice at the pressure melting point and should be included in future estimates. Hydraulic potential analysis reveals meltwater drainage pathways and their relative probability, which maps water discharge from subglacial lakes and basal melt from the upper regions of ice-flow catchments, as well as highlighting regions potentially sensitive to ice dome migration. Our analysis indicates widespread potential for subglacial lakes in the region, which coincide with over half of the lake locations proposed in previous work and identify potential locations of undetected lakes. This uncertainty-constrained drainage analysis and GHF adjustment approach is useful in the Dome Fuji region and could be applied elsewhere to diagnose basal conditions and delineate 1.5 Ma old ice.

Acknowledgments

This work is supported by funding from the Research Council of Norway (FRINATEK 315246) and is a contribution to EU Horizon 2020 Beyond EPICA Oldest Ice Core (BE-OIC) project (Grant number 815384). CReSIS radar data used in this study were collected with financial contributions from the Norwegian Polar Institute and National Institute of Polar Research, Research Organisation of Information and Systems, as a collaborative project with The University of Alabama and the University of Kansas. We acknowledge the use of the CReSIS toolbox from CReSIS generated with support from the University of Kansas, NASA Operation IceBridge grant NNX16AH54G, and NSF grants ACI-1443054, OPP-1739003, and IIS-1838230. This is BE-OI contribution number XX.

Data availability

The ice thickness, bed elevation, and topographic adjustments to geothermal heat flow grids produced by our analysis are available as GeoTIFFs from the Norwegian Polar Data Centre (https://doi.org/10.21334/npolar.2023.dbd63194). All radar-derived ice thickness datasets used in this analysis are publicly available (see *Supporting Information S1.1* for access details). Code used for geospatial analysis and stochastic simulations was adapted from open-source python packages and is described in Supporting Information S1.2.

References

Ageta, Y., Azuma, Y., Fujii, Y., Fujino, K., Fujita, S., Furukawa, T., Hondoh, T., Kameda, T., Kamiyama, K., Katagiri, K., Kawada, K., Kawamura, T., Kobayashi, S., Mae, S., Maeno, H., Miyahara, T., Motoyama, H., Nakayama, Y., Naruse, R., … Watanabe, O. (1998). Deep ice-core drilling at Dome Fuji and glaciological studies in east Dronning Maud Land, Antarctica. *Annals of Glaciology*, *27*, 333–337. doi.org/10.3189/1998aog27-1-333-337

An, M., Wiens, D. A., Zhao, Y., Feng, M., Nyblade, A., Kanao, M., Li, Y., Maggi, A., & Lévêque, J.-J. (2015). Temperature, lithosphere-asthenosphere boundary, and heat flux beneath the Antarctic Plate inferred from seismic velocities. *Journal of Geophysical Research: Solid Earth*, *120*(12), 8720–8742. doi.org/10.1002/2015JB011917

Bell, R. E., Ferraccioli, F., Creyts, T. T., Braaten, D., Corr, H., Das, I., Damaske, D., Frearson, N., Jordan, T., Rose, K., Studinger, M., & Wolovick, M. (2011). Widespread Persistent Thickening of the East Antarctic Ice Sheet by Freezing from the Base. *Science*, *331*(6024), 1592–1595. doi.org/10.1126/science.1200109

Burton-Johnson, A., Dziadek, R., & Martin, C. (2020). Review article: Geothermal heat flow in Antarctica: Current and future directions. *The Cryosphere*, *14*, 3843–3873. doi.org/10.5194/tc-14-3843-2020

Colgan, W., MacGregor, J. A., Mankoff, K. D., Haagenson, R., Rajaram, H., Martos, Y. M., Morlighem, M., Fahnestock, M. A., & Kjeldsen, K. K. (2021). Topographic Correction of Geothermal Heat Flux in Greenland and Antarctica. *Journal of Geophysical Research: Earth Surface*, *126*(2). doi.org/10.1029/2020JF005598

CReSIS Toolbox (3.0.1). (2021). [Software]. Centre for Remote Sensing of Ice Sheets (CReSIS). doi.org/10.5281/zenodo.5683959

Deutsch, C. V., & Journel, A. G. (1997). GSLIB: *Geostatistical software library and user's guide*. (Second Edition). New York: Oxford University Press.

Dow, C. F., Ross, N., Jeofry, H., Siu, K., & Siegert, M. J. (2022). Antarctic basal environment shaped by high-pressure flow through a subglacial river system. *Nature Geoscience*, 1–7. doi.org/10.1038/s41561-022-01059-1

Eagles, G., Ruppel, A., Jokat, W., & Läufer, A. (2021). *GEA IV 2013-15 radar ice thickness in eastern Dronning Maud Land* [Data set]. PANGAEA. doi.pangaea.de/10.1594/PANGAEA.938357

Eisen, O., Steinhage, D., Karlsson, N. B., Binder, T., & Helm, V. (2020). *Ice thickness of Dome Fuji region, Antarctica, recorded with the AWI airborne radar system: Line 20172023* [Data set]. PANGAEA. doi.pangaea.de/10.1594/PANGAEA.920619

Fischer, H., Severinghaus, J., Brook, E., Wolff, E., Albert, M., Alemany, O., Arthern, R., Bentley, C., Blankenship, D., Chappellaz, J., Creyts, T., Dahl-Jensen, D., Dinn, M., Frezzotti, M., Fujita, S., Gallee, H., Hindmarsh, R., Hudspeth, D., Jugie, G., … Wilhelms, F. (2013). Where to find 1.5 million yr old ice for the IPICS 'Oldest-Ice' ice core. *Climate of the Past*, *9*(6), 2489–2505. doi.org/10.5194/cp-9-2489-2013

Frémand, A. C., Fretwell, P., Bodart, J., Pritchard, H. D., Aitken, A., Bamber, J. L., Bell, R., Bianchi, C., Bingham, R. G., Blankenship, D. D., Casassa, G., Catania, G., Christianson, K., Conway, H., Corr, H. F. J., Cui, X., Damaske, D., Damm, V., Drews, R., … Zirizzotti, A. (2022). Antarctic Bedmap data: FAIR sharing of 60 years of ice bed, surface and thickness data. *Earth System Science Data Discussions*, 1–25. doi.org/10.5194/essd-2022-355

Fretwell, P., Pritchard, H. D., Vaughan, D. G., Bamber, J. L., Barrand, N. E., Bell, R., Bianchi, C., Bingham, R. G., Blankenship, D. D., Casassa, G., Catania, G., Callens, D., Conway, H., Cook, A. J., Corr, H. F. J., Damaske, D., Damm, V., Ferraccioli, F., Forsberg, R., … Zirizzotti, A. (2013). Bedmap2: Improved ice bed, surface and thickness datasets for Antarctica. *Cryosphere*, *7*(1), 375–393. doi.org/10.5194/tc-7-375-2013

Fujita, S., Holmlund, P., Matsuoka, K., Enomoto, H., Fukui, K., Nakazawa, F., Sugiyama, S., & Surdyk, S. (2012). Radar diagnosis of the subglacial conditions in Dronning Maud Land, East Antarctica. *The Cryosphere*, *6*(5), 1203–1219. doi.org/10.5194/tc-6-1203-2012

Fujita, S., Maeno, H., & Matsuoka, K. (2006). Radio-wave depolarization and scattering within ice sheets: A matrix-based model to link radar and ice-core measurements and its application. *Journal of Glaciology*, *52*(178), 407–424. doi.org/10.3189/172756506781828548

Graham, F. S., Roberts, J. L., Galton-Fenzi, B. K., Young, D., Blankenship, D., & Siegert, M. J. (2017). A high-resolution synthetic bed elevation grid of the Antarctic continent. *Earth System Science Data*, *9*(1), 267–279. doi.org/10.5194/essd-9-267-2017

Hondoh, T., Shoji, H., Watanabe, O., Salamatin, A. N., & Lipenkov, V. Y. (2002). Depth–age and temperature prediction at Dome Fuji station, East Antarctica. *Annals of Glaciology*, *35*, 384–390. doi.org/10.3189/172756402781817013

438 Howat, I. M., Porter, C., Smith, B. E., Noh, M.-J., & Morin, P. (2019). The Reference Elevation
439 Model of Antarctica. *The Cryosphere*, *13*(2), 665–674. doi.org/10.5194/tc-13-665-2019

440 Kapitsa, A. P. (1964). New data on ice thickness in the central regions of Antarctica. *Soviet*
441 *Antarctic Expedition Bulletin*, *2*, 247–250.

442 Karlsson, N. B., Binder, T., Eagles, G., Helm, V., Pattyn, F., Liefferinge, B. V., & Eisen, O.
443 (2018). Glaciological characteristics in the Dome Fuji region and new assessment for
444 'Oldest Ice'. *Cryosphere*, *12*(7), 2413–2424. doi.org/10.5194/tc-12-2413-2018

445 Kawamura, K., Abe-Ouchi, A., Motoyama, H., Ageta, Y., Aoki, S., Azuma, N., Fujii, Y., Fujita,
446 K., Fujita, S., Fukui, K., Furukawa, T., Furusaki, A., Goto-Azuma, K., Greve, R.,
447 Hirabayashi, M., Hondoh, T., Hori, A., Horikawa, S., Horiuchi, K., … Yoshimoto, T.
448 (2017). State dependence of climatic instability over the past 720,000 years from
449 Antarctic ice cores and climate modeling. *Science Advances*, *3*(2), e1600446.
450 doi.org/10.1126/sciadv.1600446

451 Kawamura, K., Nakazawa, T., Aoki, S., Sugawara, S., Fujii, Y., & Watanabe, O. (2003).
452 Atmospheric CO2 variations over the last three glacial'interglacial climatic cycles
453 deduced from the Dome Fuji deep ice core, Antarctica using a wet extraction technique.
454 *Tellus B: Chemical and Physical Meteorology*, *55*(2), 126–137.
455 doi.org/10.3402/tellusb.v55i2.16730

456 Law, R., Christoffersen, P., MacKie, E., Cook, S., Haseloff, M., & Gagliardini, O. (2023).
457 Complex motion of Greenland Ice Sheet outlet glaciers with basal temperate ice. *Science*
458 *Advances*, *9*(6), eabq5180. doi.org/10.1126/sciadv.abq5180

459 Livingstone, S. J., Li, Y., Rutishauser, A., Sanderson, R. J., Winter, K., Mikucki, J. A.,
460 Björnsson, H., Bowling, J. S., Chu, W., Dow, C. F., Fricker, H. A., McMillan, M., Ng, F.
461 S. L., Ross, N., Siegert, M. J., Siegfried, M., & Sole, A. J. (2022). Subglacial lakes and
462 their changing role in a warming climate. *Nature Reviews Earth & Environment*, 1–19.
463 doi.org/10.1038/s43017-021-00246-9

464 Lösing, M., & Ebbing, J. (2021). Predicting Geothermal Heat Flow in Antarctica With a
465 Machine Learning Approach. *Journal of Geophysical Research: Solid Earth*, *126*(6),
466 e2020JB021499. doi.org/10.1029/2020JB021499

467 MacKie, E. J., Schroeder, D. M., Caers, J., Siegfried, M. R., & Scheidt, C. (2020). Antarctic
468 Topographic Realizations and Geostatistical Modeling Used to Map Subglacial Lakes.
469 *Journal of Geophysical Research: Earth Surface*, *125*(3), e2019JF005420.
470 doi.org/10.1029/2019JF005420

471 MacKie, E. J., Schroeder, D. M., Zuo, C., Yin, Z., & Caers, J. (2021). Stochastic modeling of
472 subglacial topography exposes uncertainty in water routing at Jakobshavn Glacier.
473 *Journal of Glaciology*, *67*(261), 75–83. doi.org/10.1017/jog.2020.84

474 MacKie, E., Field, M., Wang, L., Yin, Z., Schoedl, N., & Hibbs, M. (2022). [Software]
475 *GStatSim*. Zenodo. doi.org/10.5281/zenodo.7230276

476 Martos, Y. M., Catalán, M., Jordan, T. A., Golynsky, A., Golynsky, D., Eagles, G., & Vaughan,
477 D. G. (2017). Heat Flux Distribution of Antarctica Unveiled. *Geophysical Research*
478 *Letters*, *44*(22), 11,417-11,426. doi.org/10.1002/2017GL075609

McCormack, F. S., Roberts, J. L., Dow, C. F., Stål, T., Halpin, J. A., Reading, A. M., & Siegert, M. J. (2022). Fine-Scale Geothermal Heat Flow in Antarctica Can Increase Simulated Subglacial Melt Estimates. *Geophysical Research Letters*, *49*(15), e2022GL098539. doi.org/10.1029/2022GL098539

Mälicke, M., Möller, E., Schneider, H. D., & Müller, S. (2021). [Software] scikit-gstat: A scipy flavoured geostatistical variogram analysis toolbox. *Zenodo*. doi.org/10.5281/zenodo.4835779

Mony, L., Roberts, J. L., & Halpin, J. A. (2020). Inferring geothermal heat flux from an ice-borehole temperature profile at Law Dome, East Antarctica. *Journal of Glaciology*, *66*(257), 509–519. doi.org/10.1017/jog.2020.27

Morlighem, M., Rignot, E., Binder, T., Blankenship, D., Drews, R., Eagles, G., Eisen, O., Ferraccioli, F., Forsberg, R., Fretwell, P., Goel, V., Greenbaum, J. S., Gudmundsson, H., Guo, J., Helm, V., Hofstede, C., Howat, I., Humbert, A., Jokat, W., … Young, D. A. (2020). Deep glacial troughs and stabilizing ridges unveiled beneath the margins of the Antarctic ice sheet. *Nature Geoscience*, *13*(2), Article 2. doi.org/10.1038/s41561-019-0510-8

Motoyama, H., Takahashi, A., Tanaka, Y., Shinbori, K., Miyahara, M., Yoshimoto, T., Fujii, Y., Furusaki, A., Azuma, N., Ozawa, Y., Kobayashi, A., & Yoshise, Y. (2021). Deep ice core drilling to a depth of 3035.22 m at Dome Fuji, Antarctica in 2001–07. *Annals of Glaciology*, *62*(85–86), 212–222. doi.org/10.1017/aog.2020.84

Parrenin, F., Dreyfus, G., Durand, G., Fujita, S., Gagliardini, O., Gillet, F., Jouzel, J., Kawamura, K., Lhomme, N., Masson-Delmotte, V., Ritz, C., Schwander, J., Shoji, H., Uemura, R., Watanabe, O., & Yoshida, N. (2007). 1-D-ice flow modelling at EPICA Dome C and Dome Fuji, East Antarctica. *Climate of the Past*, *3*(2), 243–259. doi.org/10.5194/cp-3-243-2007

Pattyn, F. (2010). Antarctic subglacial conditions inferred from a hybrid ice sheet/ice stream model. *Earth and Planetary Science Letters*, *295*(3), 451–461. doi.org/10.1016/j.epsl.2010.04.025

Popov, S. V., & Masolov, V. N. (2007). Forty-seven new subglacial lakes in the 0–110° E sector of East Antarctica. *Journal of Glaciology*, *53*(181), 289–297. doi.org/10.3189/172756507782202856

Purucker, M. (2012). Geothermal heat flux data set based on low resolution observations collected by the CHAMP satellite between 2000 and 2010, and produced from the MF-6 model following the technique described in Fox Maule et al. (2005). http://websrv.cs.umt.edu/isis/index.php/Main_Page

Pyrcz, M., Jo, H., Kupenko, A., Liu, W., Gigliotti, A. E., Salomaki, T., & Javier, S. (2021). [Software] *GeostatsPy: Geostatistical Library in Python* (1.0.0). doi.org/10.5281/zenodo.

Reading, A. M., Stål, T., Halpin, J. A., Lösing, M., Ebbing, J., Shen, W., McCormack, F. S., Siddoway, C. S., & Hasterok, D. (2022). Antarctic geothermal heat flow and its implications for tectonics and ice sheets. *Nature Reviews Earth & Environment*, 1–18. doi.org/10.1038/s43017-022-00348-y

Riley, S. J., DeGloria, S. D., & Elliot, R. (1999). Index that quantifies topographic heterogeneity. *Intermountain Journal of Sciences*, *5*(1–4), 23–27.

Rodriguez-Morales, F., Braaten, D., Mai, H. T., Paden, J., Gogineni, P., Yan, J. B., Abe-Ouchi, A., Fujita, S., Kawamura, K., Tsutaki, S., Liefferinge, B. V., Matsuoka, K., & Steinhage, D. (2020). A Mobile, Multichannel, UWB Radar for Potential Ice Core Drill Site Identification in East Antarctica: Development and First Results. *IEEE Journal of Selected Topics in Applied Earth Observations and Remote Sensing*, *13*, 4836–4847. doi.org/10.1109/JSTARS.2020.3016287

Shackleton, C., Matsuoka, K., Moholdt, G., Paden, J., & Van Liefferinge, B. (2023). Ice thickness, bed elevation, and topographic adjustments to geothermal heat flow near Dome Fuji, East Antarctica [Data set]. *Norwegian Polar Institute*. doi.org/10.21334/NPOLAR.2023.DBD63194

Shen, W., Wiens, D. A., Lloyd, A. J., & Nyblade, A. A. (2020). A Geothermal Heat Flux Map of Antarctica Empirically Constrained by Seismic Structure. *Geophysical Research Letters*, *47*(14), e2020GL086955. doi.org/10.1029/2020GL086955

Shreve, R. L. (1972). The movement of water in glaciers. *Journal of Glaciology*, *11*(62), 205–214.

Siegert, M. J. (2000). Antarctic subglacial lakes. *Earth Science Reviews*, *50*(1–2), 29–50. doi.org/10.1016/S0012-8252(99)00068-9

Stål, T., Reading, A. M., Halpin, J. A., & Whittaker, J. M. (2021). Antarctic Geothermal Heat Flow Model: Aq1. *Geochemistry, Geophysics, Geosystems*, *22*(2), e2020GC009428. doi.org/10.1029/2020GC009428

Talalay, P., Yazhou, L., Augustin, L., Clow, G., Hong, J., Lefebvre, E., Markov, A., Motoyama, H., & Ritz, C. (2020). Geothermal heat flux from measured temperature profiles in deep ice boreholes in Antarctica. *The Cryosphere*, *14*, 4021–4037. doi.org/10.5194/tc-14-4021-2020

Tarboton, D. G. (1997). A new method for the determination of flow directions and upslope areas in grid digital elevation models. *Water Resources Research*, *33*(2), 309–319. doi.org/10.1029/96WR03137

Tsutaki, S., Fujita, S., Kawamura, K., Abe-Ouchi, A., Fukui, K., Motoyama, H., Hoshina, Y., Nakazawa, F., Obase, T., Ohno, H., Oyabu, I., Saito, F., Sugiura, K., & Suzuki, T. (2021a). Ice thickness around Dome Fuji, Antarctica, based on JARE ground-based radar surveys: JARE33 data. *Arctic Data Archive System (ADS)*, *1.00*(Japan). http://doi.org/10.17592/001.2021110909

Tsutaki, S., Fujita, S., Kawamura, K., Abe-Ouchi, A., Fukui, K., Motoyama, H., Hoshina, Y., Nakazawa, F., Obase, T., Ohno, H., Oyabu, I., Saito, F., Sugiura, K., & Suzuki, T. (2021b). Ice thickness around Dome Fuji, Antarctica, based on JARE ground-based radar surveys: JARE37 data. *Arctic Data Archive System (ADS)*, *1.00*(Japan). http://doi.org/10.17592/001.2021110909

Tsutaki, S., Fujita, S., Kawamura, K., Abe-Ouchi, A., Fukui, K., Motoyama, H., Hoshina, Y., Nakazawa, F., Obase, T., Ohno, H., Oyabu, I., Saito, F., Sugiura, K., & Suzuki, T. (2021c). Ice thickness around Dome Fuji, Antarctica, based on JARE ground-based radar

surveys: JARE40 data. *Arctic Data Archive System (ADS)*, *1.00*(Japan). http://doi.org/10.17592/001.2021110909

Tsutaki, S., Fujita, S., Kawamura, K., Abe-Ouchi, A., Fukui, K., Motoyama, H., Hoshina, Y., Nakazawa, F., Obase, T., Ohno, H., Oyabu, I., Saito, F., Sugiura, K., & Suzuki, T. (2021d). Ice thickness around Dome Fuji, Antarctica, based on JARE ground-based radar surveys: JARE49 POL 179 MHz data. *Arctic Data Archive System (ADS)*, *1.00*(Japan). http://doi.org/10.17592/001.2021110909

Tsutaki, S., Fujita, S., Kawamura, K., Abe-Ouchi, A., Fukui, K., Motoyama, H., Hoshina, Y., Nakazawa, F., Obase, T., Ohno, H., Oyabu, I., Saito, F., Sugiura, K., & Suzuki, T. (2021e). Ice thickness around Dome Fuji, Antarctica, based on JARE ground-based radar surveys: JARE49 VHF 60 MHz data. *Arctic Data Archive System (ADS)*, *1.00*(Japan). http://doi.org/10.17592/001.2021110909

Tsutaki, S., Fujita, S., Kawamura, K., Abe-Ouchi, A., Fukui, K., Motoyama, H., Hoshina, Y., Nakazawa, F., Obase, T., Ohno, H., Oyabu, I., Saito, F., Sugiura, K., & Suzuki, T. (2021f). Ice thickness around Dome Fuji, Antarctica, based on JARE ground-based radar surveys: JARE54 data. *Arctic Data Archive System (ADS)*, *1.00*(Japan). http://doi.org/10.17592/001.2021110909

Tsutaki, S., Fujita, S., Kawamura, K., Abe-Ouchi, A., Fukui, K., Motoyama, H., Hoshina, Y., Nakazawa, F., Obase, T., Ohno, H., Oyabu, I., Saito, F., Sugiura, K., & Suzuki, T. (2021g). Ice thickness around Dome Fuji, Antarctica, based on JARE ground-based radar surveys: JARE59 POL 179 MHz data. *Arctic Data Archive System (ADS)*, *1.00*(Japan). http://doi.org/10.17592/001.2021110909

Tsutaki, S., Fujita, S., Kawamura, K., Abe-Ouchi, A., Fukui, K., Motoyama, H., Hoshina, Y., Nakazawa, F., Obase, T., Ohno, H., Oyabu, I., Saito, F., Sugiura, K., & Suzuki, T. (2021h). Ice thickness around Dome Fuji, Antarctica, based on JARE ground-based radar surveys: JARE59 VHF 179 MHz data. *Arctic Data Archive System (ADS)*, *1.00*(Japan). http://doi.org/10.17592/001.2021110909

Tsutaki, S., Fujita, S., Kawamura, K., Abe-Ouchi, A., Fukui, K., Motoyama, H., Hoshina, Y., Nakazawa, F., Obase, T., Ohno, H., Oyabu, I., Saito, F., Sugiura, K., & Suzuki, T. (2021i). Ice thickness around Dome Fuji, Antarctica, based on JARE ground-based radar surveys: JARE60 data. *Arctic Data Archive System (ADS)*, *1.00*(Japan). http://doi.org/10.17592/001.2021110909

Tsutaki, S., Fujita, S., Kawamura, K., Abe-Ouchi, A., Fukui, K., Motoyama, H., Hoshina, Y., Nakazawa, F., Obase, T., Ohno, H., Oyabu, I., Saito, F., Sugiura, K., & Suzuki, T. (2022). High-resolution subglacial topography around Dome Fuji, Antarctica, based on ground-based radar surveys over 30 years. *The Cryosphere*, *16*(7), 2967–2983. doi.org/10.5194/tc-16-2967-2022

Uieda, L. (2018). Verde: Processing and gridding spatial data using Green's functions. *Journal of Open Source Software*, *3*(30), 957. doi.org/10.21105/joss.00957

van der Veen, C. J., Leftwich, T., von Frese, R., Csatho, B. M., & Li, J. (2007). Subglacial topography and geothermal heat flux: Potential interactions with drainage of the Greenland ice sheet. *Geophysical Research Letters*, *34*(12). doi.org/10.1029/2007GL030046

Van Liefferinge, B., & Pattyn, F. (2013). Using ice-flow models to evaluate potential sites of million year-old ice in Antarctica. *Climate of the Past*, *9*, 2335–2345.

Van Liefferinge, B., Pattyn, F., Cavitte, M. G. P., Karlsson, N. B., Young, D. A., Sutter, J., & Eisen, O. (2018). Promising oldest ice sites in east antarctica based on thermodynamical modelling. *Cryosphere*, *12*(8), 2773–2787. doi.org/10.5194/tc-12-2773-2018

Van Liefferinge, B., Taylor, D., Tsutaki, S., Fujita, S., Gogineni, P., Kawamura, K., Matsuoka, K., Moholdt, G., Oyabu, I., Abe-Ouchi, A., Awasthi, A., Buizert, C., Gallet, J.-C., Isaksson, E., Motoyama, H., Nakazawa, F., Ohno, H., O'Neill, C., Pattyn, F., & Sugiura, K. (2021). Surface Mass Balance Controlled by Local Surface Slope in Inland Antarctica: Implications for Ice-Sheet Mass Balance and Oldest Ice Delineation in Dome Fuji. *Geophysical Research Letters*, *48*(24), e2021GL094966. doi.org/10.1029/2021GL094966

Watanabe, O., Kamiyama, K., Motoyama, H., Fujii, Y., Shoji, H., & Satow, K. (1999). The paleoclimate record in the ice core at Dome Fuji station, East Antarctica. *Annals of Glaciology*, *29*, 176–178. doi.org/10.3189/172756499781821553

Wright, A., & Siegert, M. (2012). A fourth inventory of Antarctic subglacial lakes. *Antarctic Science*, *24*(6), 1–6. doi.org/10.1017/S095410201200048X

Zwally, H. J., Giovinetto, M. B., Beckley, M. A., & Saba, J. L. (2012). *Antarctic and Greenland Drainage Systems*. GSFC Cryospheric Sciences Laboratory; 610 Web Dev. https://earth.gsfc.nasa.gov/cryo/data/polar-altimetry/antarctic-and-greenland-drainage-systems